AFM Analysis of 3D Printing PEI for Automotive Applications

Khanh Q. Nguyen, Pascal Y. Vuillaume, Mathieu Robert, and Saïd Elkoun

Abstract In recent years, fused deposition modeling (FDM) (or 3D printing) technology is increasingly applied in the automotive industry due to its rapid operation and cheap costs. The use of high-performance polymers which can retain their good properties under high temperatures and harsh conditions, along with 3D printing techniques is, therefore, essential. Polyetherimide (PEI) is a high-performance thermoplastic that is attracting use in electrical and lighting systems for the automotive market. PEI is well-known as an amorphous thermoplastic with high heat resistance, mechanical strength, and chemical resistance. Therefore, PEI is used in transmission and ignition components, bezels, reflectors, and electromechanical systems as an alternative to metal, thermoset as well as bulk molding components. Despite many potential advantages, PEI produced from 3D printing technology has not been widely used in the automotive sector. The lack of understanding about the material degradation mechanism as well as 3D printed parts quality are challenges in the widespread application of PEI materials to automotive applications. In this study, two tensile specimens of 3D printing PEI from the FDM technique with different printing parameters were investigated. The present study aims to evaluate the interface quality and mechanical strength of 3D printed parts using atomic force microscope (AFM) analysis. Moreover, the comparison focuses on the roughness and Young's modulus between these 3D printing PEI is also highlighted.

Keywords Fused deposition modelling (FDM) and 3D printing technologies · Polyetherimide (PEI) · Automotive applications · Atomic force microscope (AFM) analysis · Interface · roughness · and Young's modulus

K. Q. Nguyen (✉) · M. Robert
Department of Civil and Building Engineering, University of Sherbrooke, 2500, boulevard de l'Université, Sherbrooke, QC J1K 2R1, Canada
e-mail: Quoc.Khanh.Nguyen@USherbrooke.ca

P. Y. Vuillaume
Center of Mineral Technology and Plastics (COALIA), Thetford Mines, QC G6G 1N1, Canada

S. Elkoun
Department of Mechanical Engineering, University of Sherbrooke, 2500, boulevard de l'Université, Sherbrooke, QC J1K 2R1, Canada

1 Introduction

Additive manufacturing (AM) is known as three-dimensional (3D) printing which gains popularity with the printing process layer upon layer. AM makes it possible to print lightweight components with complex geometries, and no need for specific molds or tools compared to conventional methods [1–3]. Among AM technologies, fused deposition modeling (FDM) is the most widely 3D printing method due to its rapid operation and cheap costs [4–7]. In addition, the thermoplastic filament is a widely used material to build 3D-printed parts. For the FDM technology, however, materials with high melting temperatures are difficult to print. These materials are called high-performance polymers which can retain their good properties under high temperatures and harsh conditions. Moreover, non-uniform layer thickness during printing is one of the significant problems for these high-performance polymers [8, 9]. Nowadays, along with technical development in FDM technology, high-performance polymers such as polyetherimide (PEI) can be printed without geometrical limitations [10]. PEI is an amorphous thermoplastic that can be used in various structural components for automotive applications as an alternative to metal, thermoset as well as bulk molding components. Electrical and lighting systems are the principal applications of PEI, including transmission and ignition components, throttle bodies, thermostat housings, bezels, reflectors, bezels, light bulb sockets, and electromechanical systems [11]. In contrast, very little has been found in the literature about 3D printing PEI for automotive applications. The lack of understanding about the material degradation mechanism and 3D printed parts quality are challenges in the widespread application of PEI materials. For 3D printing, surface quality and layer thickness are the factors that affect the quality of the final printed product [12]. It is evident that the printing parameters such as build orientation, raster angle, and printing speed [13–15] are the most influential on 3D printed parts. Contrariwise, investigative techniques and analysis of interface layer and mechanical properties at nanometric scale are limited. In this regard, the atomic force microscope (AFM) analysis, therefore, is a widely used analysis that explores all kinds of surface properties. AFM is often used to investigate the mechanical properties of the interface [16]. Furthermore, AFM is well-known as a non-destructive technique to analyze 3D printing materials [17].

In the current study, two tensile specimens of 3D printing PEI from the FDM technique with different printing parameters are investigated. The objective is to evaluate the surface quality of 3D printed parts using AFM analysis. Moreover, Young's modulus and roughness between layers of two PEI specimens are also highlighted.
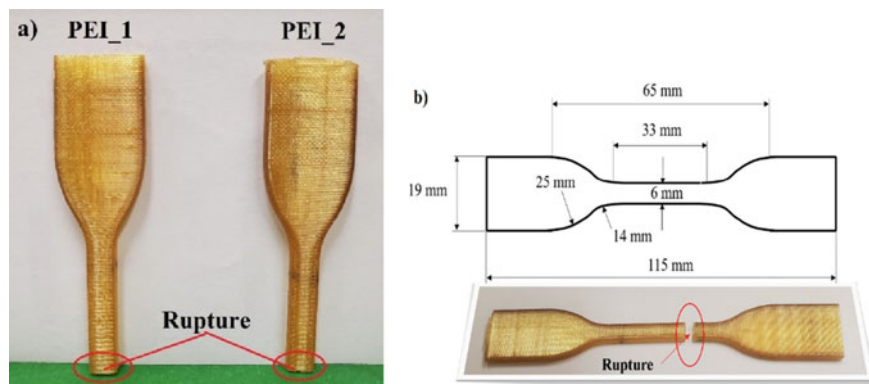
Fig. 1 Tensile specimens of PEI **a** part of the specimen after tensile tests, **b** specimens' dimension

Table 1 Properties of PEI in literature [20, 21]

Chemical formula	T_g (°C)	Tensile strength (MPa)	Young's modulus (GPa)
$(C_{37}H_{24}O_6N_2)_n$	217	104	2.96

2 Materials and Experimental Approach

2.1 Materials

A total of two tensile specimens of PEI, including PEI_1 and PEI_2, were investigated as shown in Fig. 1a. These PEI specimens were printed by the FDM technique with different printing parameters from one local manufacturer. Specimens' geometry and dimension were according to ASTM D638 [18] (standard test method for tensile properties of plastics) as illustrated in Fig. 1b [19]. In general, PEI has high thermal stability by aromatic imide units and good processability due to ether linkages. The glass transition temperature (T_g) and Young's modulus of PEI are 217 °C and 2.96 GPa [20, 21], respectively (Table 1). The surface ($6 \times 4 \times 2$ mm^3) near the rupture area after tensile tests was used for all AFM experiments.

2.2 AFM Analysis

Atomic force microscope (AFM) consists of high-resolution microscopy at the nanoscale. This technique provides information about topography (roughness, size), electrical, nanomechanical properties, and surface modification of materials. In this study, an atomic force microscope (AFM) (Nanosurf FlexAFM) combined with the C3000 controller was used for all experiments at ambient conditions (temperature ≈

25 °C). The AFM experiments were performed with a silicon probe operated in the air. The principle of AFM is based on a small probe, that is, a very thin cantilever with a tip coupled with piezoelectric elements in order to scan the surface of materials (Fig. 2). During the scan process, the interactions between the sensor tip and the sample surface atoms are converted to probe deflection/amplitude/frequency variations, which depend on the tip-to-sample distance. In addition, AFM operation is usually described in two modes, including static mode (contact mode) and dynamic mode (tapping mode/phase contrast mode). For static mode, once the force is applied, the bend of the cantilever is detected using a cantilever deflection detection system. In contrast, the cantilever is excited using a piezo element for dynamic mode. This piezo oscillated with a fixed frequency close to the free resonance frequency of the cantilever. The repulsive force acting on the tip increases the resonance frequency of the cantilever, resulting in the vibration amplitude of the cantilever decreasing. This vibration is also measured by a cantilever deflection detection system. In this paper, the phase contrast mode was used for investigating surface quality and roughness. Contrariwise, the elastic modulus was measured using static mode.

Surface Analysis and Roughness Measurements

In this study, the phase contrast mode was used to perform the surface and roughness measurements. An image of the surface was obtained by scanning over the PEI surface in the X and Y axes. The image size was 10 μm × 10 μm. The time needed to acquire a single data line was applied to 0.8 s with 250 data points per line. Moreover, the interaction between tip and surface sample was constant through the Z-controller during imagining. The working point for the Z-controller was relative cantilever vibration amplitude. In fact, a Setpoint of 60% was used. In other words, the Z-controller moved the tip closer to the surface sample until the vibration amplitude decreased to 60% of the vibration amplitude far away from the sample. It should be noted that an I-Gain value was set to 2000 in order to overcome error signals. On

Fig. 2 Diagram of an AFM probe interacting with a sample surface
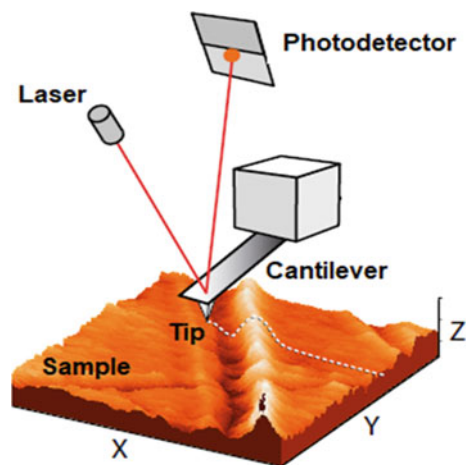
the other hand, the reference amplitude of the cantilever vibration was applied to 500 mV. That means the excitation strength was adjusted once this amplitude was reached.

Using an "approach" function, the tip was moved close to PEI surfaces. Once the imaging parameters were set, an image of the PEI surface was achieved through the "acquisition" window. The surface quality and roughness of two PEI specimens were investigated afterward.

Modulus Measurements

Very little has been found in the literature about analytical techniques for mechanical properties at nanometric scale at interface or interlayer of materials. Using Force Spectroscopy of AFM mode is, however, an approach to nanomechanical measurements on all kinds of samples, including solid and liquid [17, 22]. In the current study, "Force–Distance" curves in AFM static were used to measure Young's modulus of two PEI samples. Like instrumented indentation testing (IIT), in the Force Spectroscopy mode of AFM, the probe is used as an indenter which is driven into a specific area of materials by vertical force. In this measurement procedure, the cantilever is moved while the deflection signal is recorded.

For Force Spectroscopy, the obtained data is presented as a typical force curve (Fig. 3). If the tip is far from the surface, there is neither cantilever deflection nor interaction between the tip and the sample surface. In contrast, once the tip and sample are in contact, there are attractive or repulsive forces between them. At this point, the tip is bent up upon further movement of the z-piezo and *jump-to contact* (1) takes place. In general, the van der Waals forces are the main force that maintains this interaction between tip and surface sample. Once the maximum force is reached, the tip unbent while being withdrawn from the surface. However, the tip remains in contact with the surface for a short time by adhesion forces before fully retracting from the surface. This stage is known as *jump-off-contact* (2) illustrated in Fig. 3. In this study, a distance range of 1 μm, 1024 data points, and a maximum force of 100 nN were applied for the Force-Distance curve parameters.

3 Results and Discussions

3.1 *Surface Analysis*

The surface characterization of two PEI specimens was investigated using phase contrast imaging in the tapping mode AFM. Figure 4 shows the AFM topographic of two PEI specimens recorded from the surface near the rupture area after tensile tests. The image size was 10 μm × 10 μm. Figure 4a and c show the topographic images of PEI_1 and PEI_2, respectively. In addition, the 3D images were presented for PEI_1 and PEI_2 in Fig. 4b and d, respectively. For the PEI_1 specimen, the results show that the layers of the 3D printing process were detected. However, there were
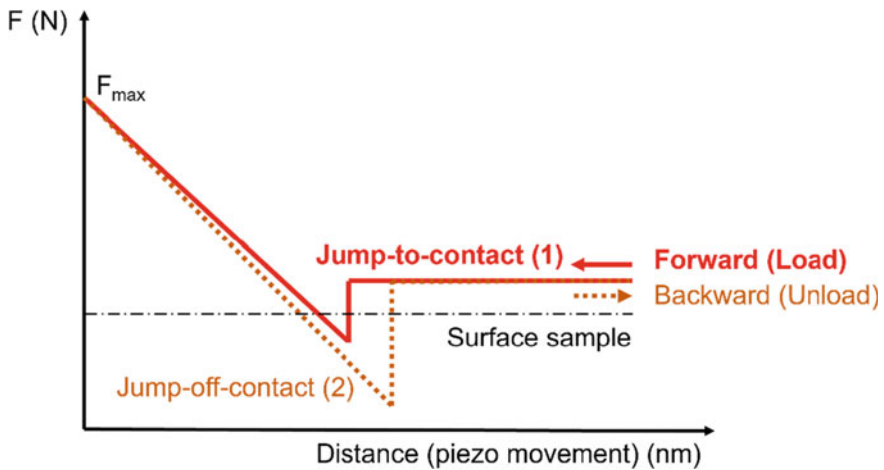
Fig. 3 Principle of AFM force spectroscopy (adapted from Roa et al. [17])

significant variations in width between layers as shown in Fig. 4a. In contrast, there were no visible layers found for the PEI_2 specimen as illustrated in Fig. 4c. That could explain that different printing processes affected topographic images. In the current study, however, these printing parameters were not available to the authors as a secret of the manufacturer.

3.2 Roughness Measurements

The surface roughness is a characteristic of the texture of a surface. It plays a key role in evaluating the potential performance of materials. It is evident that irregularities on the surface can form cracks or be the cause of materials degradation. Table 2 shows the area roughness values of PEI_1 and PEI_2 specimens. The investigated area was 100.8 pm^2 for both PEI_1 and PEI_2 specimens. This area was the same area in surface imaging AFM mode.

It is usually considering the root mean square (S_q) and the roughness average (S_a) for evaluating the roughness of materials. In the current study, the results show that the PEI_1 specimen was rougher than the PEI_2 specimen. For the PEI_2 specimen, the values of S_q and S_a were lower than those of the PEI_1 specimen. It could be pointed out that some factors such as deposition that occur during high pressure and high-temperature conditions of the printing process can increase surface roughness.
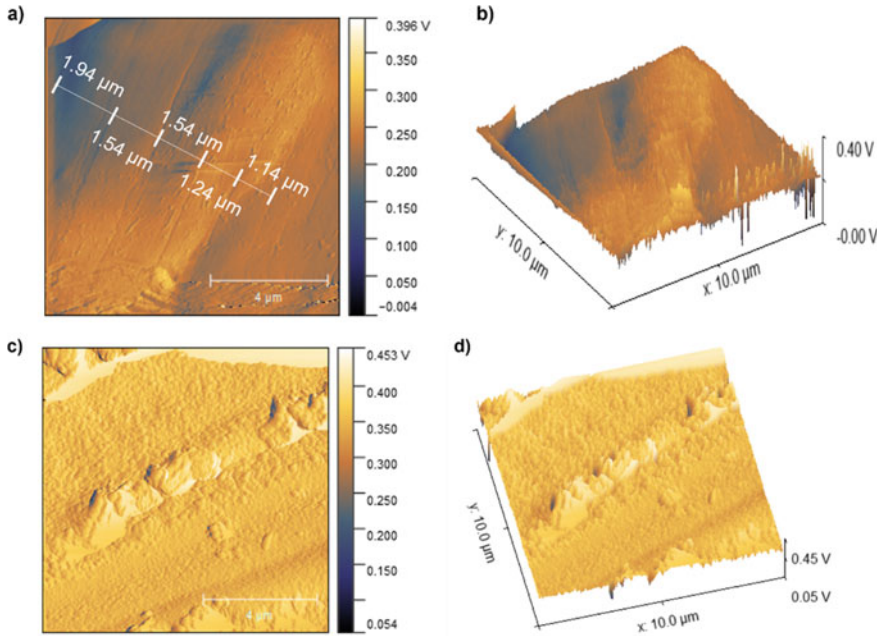
Fig. 4 Topographic images **a** PEI_1, **b** PEI_2 and 3D images, **c** PEI_1, **d** PEI_2

Table 2 Area roughness of PEI specimens

Roughness value	PEI_1	PEI_2
Roughness average (S_a) (nm)	94.17	84.27
Root mean square (S_q) (nm)	122.33	107.12
Peak-valley height (S_y) (nm)	699.44	769.33
Peak height (S_p) (nm)	292.54	424.01
Valley depth (S_v) (nm)	−406.90	−345.32
Mean value (S_m) (fm)	−21.71	−21.70

3.3 Modulus Measurements

For AFM analysis, there are many models to measure the modulus of materials such as the Hertz model, Derjaguin, Müller, and Toporov (DMT) model, Johnson, Kendall, and Roberts (JKR) model, Pyramidal Regular 4-Sided model, and Sneddon Cone model. Like the classic nanoscopic indentation experiments, the modulus is also determined based on the contact area (A_c) for the AFM technique. It should be highlighted that A_c cannot be measured directly by imaging technique but rather by Force Spectroscopy mode of AFM. In this study, the Hertz model was used to investigate the modulus of materials due to its simplicity. Both tip and sample are considered as two spheres of radius for the Hertz model. Furthermore, this model only

considers the elastic deformation and ignores the plastic deformation of materials [17]. The contact area for the Hertz model is described as Eq. (1).

$$A_c = \pi \left(\frac{RF}{K} \right)^{2/3}$$

(1)

where, A_c is the contact area; R is the combined curvature radius of the contact; F is the force; K is the combined elastic modulus of different materials as given by Eq. (2).

$$K = \frac{4}{3} \left(\frac{1 - \vartheta_i^2}{E_i} + \frac{1 - \vartheta^2}{E} \right)^{-1}$$

(2)

where, E is Young's modulus; ϑ is Poisson's ratio.

In the current study, the square size was 9.49 μm for the PEI_1 specimen, and 9.69 μm for the PEI_2 specimen. The grid size of 8 × 8, the Poisson's ratio of 0.5, and the tip radius of 10 nm were applied to measure Young's modulus of two PEI specimens.

Figure 5a and b show Young's modulus of PEI_1 and PEI_2 specimens, respectively. By integrating Flex-ANA software with AFM analysis, Young's modulus values at each area (1×1 μm^2) scanned over the surface area of both specimens PEI_1 and PEI_2 were easily addressed as shown in Fig. 5. Therefore, modulus values at different locations on the surface could be determined. In other words, the modulus value at the layer-to-layer interface of the 3D printed material could be measured by AFM analysis. Moreover, Young's modulus value of specimen PEI_2 was higher than those of specimen PEI_1. This result is consistent with the roughness of specimen PEI_2 which was lower than that of specimen PEI_1. Specifically, the mean Young's modulus of specimens PEI_1 and PEI_2 were 620 MPa and 2300 MPa, respectively. Therefore, the PEI_2 printed specimen may be suitable for automotive applications rather than the PEI_1 specimen due to its modulus being similar to the reference value (2930 MPa) [20, 21].

4   Conclusions

In this study, the AFM analysis has been successfully applied to investigate the surface quality, roughness, and Young's modulus of two 3D printed parts. These specimens of 3D printing, including PEI_1 and PEI_2 from the FDM technique used in automotive applications, were investigated. The results show that there were significant variations in width between layers for the PEI_1 specimen. In contrast, there were no visible layers found for the PEI_2 specimen. It's interesting to point out that printing processes affected topographic images. The PEI_2 specimen had a lower root mean square (S_q) and roughness average (S_a) for roughness measurement
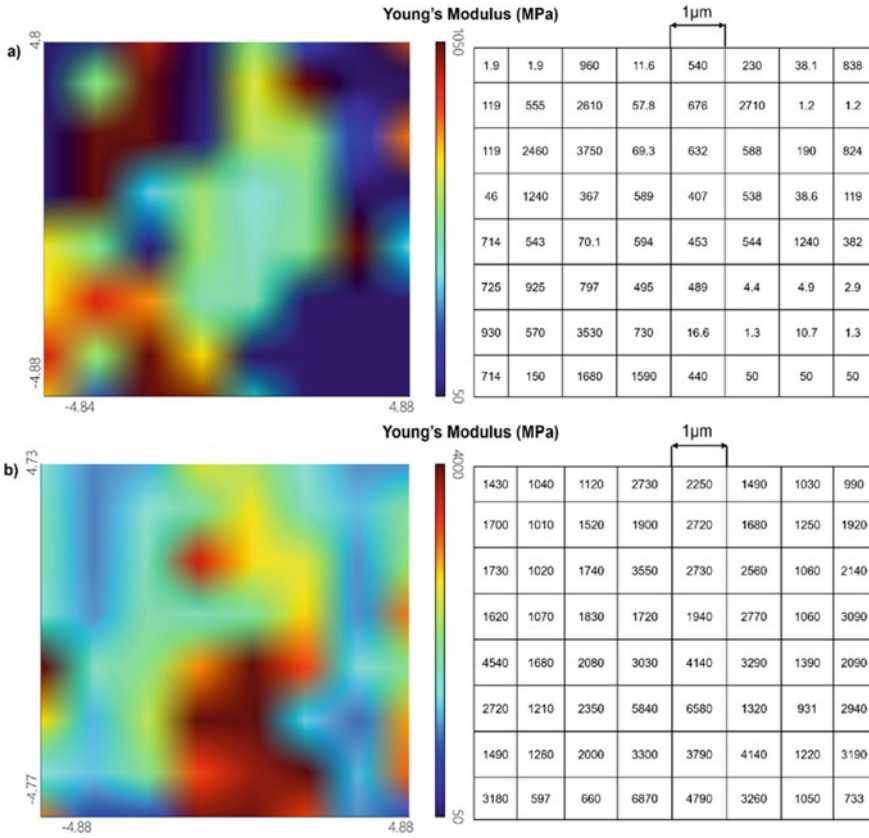
Fig. 5 Young's modulus of PEI specimens **a** PEI_1, **b** PEI_2

than the PEI_1 specimen. As a result, the PEI_1 specimen was rougher than the PEI_2 specimen. It could be pointed out that some factors such as deposition that occur during high-pressure and high-temperature conditions of the printing process can increase surface roughness. Moreover, Young's modulus value of specimen PEI_2 was higher than those of specimen PEI_1. It can be concluded that the PEI_2 printed specimen may be suitable for automotive applications due to its modulus being similar to the reference value (2930 MPa). However, further studies on how to determine Young's modulus of materials by the AFM technique should be conducted in the future. The application of the DMT, JKR, Pyramidal Regular 4-Sided, and Sneddon Cone models is essential. The choice of which model is suitable for each specific material should be investigated.

References

1. Ahn S, Montero M, Odell D, Roundy S, Wright PK (2002) Anisotropic material properties of fused deposition modeling ABS. Rapid Prototyp J 8(4):248–257. https://doi.org/10.1108/135 52540210441166
2. Weller C, Kleer R, Piller FT (2015) Economic implications of 3D printing: market structure models in light of additive manufacturing revisited. Int J Prod Econ 164:43–56. https://doi.org/ 10.1016/j.ijpe.2015.02.020
3. Schniederjans DG (2017) Adoption of 3D-printing technologies in manufacturing: a survey analysis. Int J Prod Econ 183:287–298. https://doi.org/10.1016/j.ijpe.2016.11.008
4. Calignano F, Manfredi D, Ambrosio EP, Biamino S, Lombardi M, Atzeni E, Fino P (2017) Overview on additive manufacturing technologies. Proc IEEE 105(4):593–612. https://doi.org/ 10.1109/JPROC.2016.2625098
5. Martínez J, Diéguez JL, Ares E, Pereira A, Hernández P, Pérez JA (2013) Comparative between FEM models for FDM parts and their approach to a real mechanical behaviour. Procedia Eng 63:878–884. https://doi.org/10.1016/j.proeng.2013.08.230
6. Stansbury JW, Idacavage MJ (2016) 3D printing with polymers: challenges among expanding options and opportunities. Dent Mater 32(1):54–64. https://doi.org/10.1016/j.dental.2015. 09.018
7. Ford S, Despeisse M (2016) Additive manufacturing and sustainability: an exploratory study of the advantages and challenges. J Clean Prod 137:1573–1587. https://doi.org/10.1016/j.jcl epro.2016.04.150
8. Vasudevarao B, Natarajan DP, Henderson M, Razdan A (2000) Sensitivity of RP surface finish to process parameter variation 251. https://doi.org/10.26153/TSW/3045
9. Anitha R, Arunachalam S, Radhakrishnan P (2001) Critical parameters influencing the quality of prototypes in fused deposition modelling. J Mater Process Technol 118(1–3):385–388. https:/ /doi.org/10.1016/S0924-0136(01)00980-3
10. Vanaei S, Parizi MS, Vanaei S, Salemizadehparizi F, Vanaei HR (2021) An overview on materials and techniques in 3D bioprinting toward biomedical application. Eng Regen 2:1–18. https:/ /doi.org/10.1016/j.engreg.2020.12.001
11. Omnexus (2022) Polyetherimide (PEI) polymer: uses, applications and material properties. https://omnexus.specialchem.com/selection-guide/polyetherimide-pei-high-heat-plastic/ key-features-applications-of-pei. Accessed 13 Sept 2022
12. Gómez-Gras G, Pérez MA, Fábregas-Moreno J, Reyes-Pozo G (2021) Experimental study on the accuracy and surface quality of printed versus machined holes in PEI Ultem 9085 FDM specimens. Rapid Prototyp J 27(11):1–12. https://doi.org/10.1108/RPJ-12-2019-0306
13. Mohamed O, Masood S, Bhowmik J (2016) Analytical modelling and optimization of the temperature-dependent dynamic mechanical properties of fused deposition fabricated parts made of PC-ABS. Materials 9(11):895. https://doi.org/10.3390/ma9110895
14. Rodríguez-Panes A, Claver J, Camacho A (2018) The influence of manufacturing parameters on the mechanical behaviour of PLA and ABS pieces manufactured by FDM: a comparative analysis. Materials 11(8):1333. https://doi.org/10.3390/ma11081333
15. Solomon IJ, Sevvel P, Gunasekaran J (2021) A review on the various processing parameters in FDM. Mater Today Proc 37:509–514. https://doi.org/10.1016/j.matpr.2020.05.484
16. Monclus MA, Young TJ, Di Maio D (2010) AFM indentation method used for elastic modulus characterization of interfaces and thin layers. J Mater Sci 45(12):3190–3197. https://doi.org/ 10.1007/s10853-010-4326-6
17. Roa JJ, Oncins G, Diaz J, Sanz F, Segarra M (2011) Calculation of Young's modulus value by means of AFM. Recent Pat Nanotechnol 5(1):27–36. https://doi.org/10.2174/187221011794 474985
18. ASTM D638 (2014) Standard test methods for tensile properties of plastics. ASTM International, West Conshohocken, PA, USA

19. Nguyen KQ, Cousin P, Mohamed K, Robert M, Benmokrane B (2022) Effects of exposure conditions on antioxidant depletion, tensile strength, and creep modulus of corrugated HDPE pipes made with or without recycled resins. J Polym Environ 1–15. https://doi.org/10.1007/s10924-022-02487-1
20. Shibata M, Fang Z, Yosomiya R (2001) Miscibility and crystallization behavior of poly(ether ether ketone ketone)/poly(ether imide) blends. J Appl Polym Sci 80(5):769–775. https://doi.org/10.1002/1097-4628(20010502)80:5%3c769::AID-APP1153%3e3.0.CO;2-B
21. El Magri A, Vanaei S, Vaudreuil S (2021) An overview on the influence of process parameters through the characteristic of 3D-printed PEEK and PEI parts. High Perform Polym 33(8):862–880. https://doi.org/10.1177/09540083211009961
22. Fraxedas J, Garcia-Manyes S, Gorostiza P, Sanz F (2002) Nanoindentation: toward the sensing of atomic interactions. Proc Natl Acad Sci 99(8):5228–5232. https://doi.org/10.1073/pnas.042106699